Journal of the Physical Society of Japan **80** (2011) 084703 **FULL PAPERS**
DOI: 10.1143/JPSJ.80.084703

Local Valence Electronic States of SiO_2 Ultrathin Films Grown on Si(100) Studied Using Auger Photoelectron Coincidence Spectroscopy: Observation of Upward Shift of Valence-Band Maximum as a Function of SiO_2 Thickness

Takuhiro KAKIUCHI[1*], Narihiko FUJITA[2], Kazuhiko MASE[1,3], Masatoshi TANAKA[2], and Shin-ichi NAGAOKA[4]

[1]*Department of Materials Structure Science, School of High Energy Accelerator Science, The Graduate University for Advanced Studies, Tsukuba, Ibaraki 305-0801, Japan*
[2]*Department of Physics, Faculty of Engineering, Yokohama National University, Yokohama 240-8501, Japan*
[3]*Institute of Materials Structure Science, KEK, Tsukuba, Ibaraki 305-0801, Japan*
[4]*Department of Chemistry, Faculty of Science, Ehime University, Matsuyama 790-8577, Japan*

(Received January 18, 2011; accepted June 2, 2011; published online July 25, 2011)

The local valence electronic states of the surface, interface, and substrate for SiO_2 ultrathin films thermally grown on a Si(100)-2×1 have been investigated using Si-$L_{23}VV$ Auger-electron Si^{n+}-2p photoelectron coincidence spectroscopy (n represents the number of oxygen atoms bonded to the Si). A series of Si-$L_{23}VV$ Auger electron spectra (AES) measured in coincidence with Si^{n+}-2p photoelectron indicate that the valence electronic states in the vicinity of the Si^{n+} sites shift to the deeper binding-energy side as n increases. Furthermore, the Si^{4+}-$L_{23}VV$ AES measured as a function of the thickness of the SiO_2, show that the valence-band maximum of SiO_2 shifts ~1.6 eV toward the Fermi level when the thickness of the SiO_2 film is decreased to 1.7–1.5 Å. This shift is attributed to a decrease in the number of Si^{4+} and an increase in the number of Si^{3+}, Si^{2+}, Si^{1+}, and Si^0 in the vicinity of the topmost SiO_2 layer.

KEYWORDS: local valence electronic structure, valence-band maximum, band-gap narrowing, SiO_2 ultrathin film, Si(100), Auger photoelectron coincidence spectroscopy (APECS), Auger electron spectroscopy, photoelectron spectroscopy, synchrotron radiation, metal–oxide–semiconductor field-effect transistors

1. Introduction

The local valence electronic states of SiO_2 ultrathin films grown on a Si(100)-2×1 surface [SiO_2/Si(100)] have been studied extensively because (1) in-depth understanding of the electronic properties of surfaces and interfaces from an atomic point of view is of fundamental importance in science, and (2) these films play dominant roles in metal–oxide–semiconductor field-effect transistors (MOSFETs). The oxidation processes, atomic structures, and chemical compositions of the surface, interface, and substrate in the case of SiO_2/Si(100) are closely related to the local valence electronic states, and have been investigated in detail over the last three decades. The following findings have been reported: 1) a SiO_2 film can be grown thermally on Si(100) in the layer-by-layer mode to form an amorphous structure;[1)] 2) the SiO_2/Si(100) interface is abrupt (<5 Å) and contains partially oxidized silicon (Si^{n+}, $n = 1, 2, 3$, where n represents the number of oxygen atoms bonded to the Si atom);[2)] and 3) Si or SiO desorption is induced at the SiO_2/Si(100) interface by the stress resulting from lattice mismatch between the SiO_2 thin film and the Si substrate.[3–5)] In this paper, we report a site-selective study of the local valence electronic states of the surfaces and interfaces for SiO_2/Si(100) carried out by using Si-$L_{23}VV$ Auger-electron Si^{n+}-2p photoelectron coincidence spectroscopy. Auger photoelectron coincidence spectroscopy (APECS) is a unique method used to measure an Auger electron spectrum derived from a specific photoemission.[6–10)] In particular, core–valence–valence (CVV) APECS is used to investigate the local valence electronic structures of surfaces in a site-selective manner.[11,12)]

Ultraviolet photoelectron spectroscopy (UPS) is the most standard technique used for studying the valence electronic states of SiO_2/Si(100),[13)] but it is difficult to obtain information on the local electronic states of surfaces or interfaces by using this technique. Soft-X-ray emission spectroscopy (SXES), in which tunable synchrotron radiation (SR) is used, is an effective tool for probing the local valence electronic states of a particular atom in a specific chemical environment. Using SXES, Yamashita *et al.* observed that the local valence electronic states projected to the O site at the SiO_2/Si interface shift upward in comparison with those in bulk SiO_2.[14)] Electron energy-loss spectroscopy (EELS) measurements carried out in a scanning transmission electron microscope with a beam diameter of 0.2–0.5 nm also aid the investigation of local valence electronic states. Using EELS, Muller *et al.* observed that the conduction-band minimum (CBM) of the O site at the SiO_2/Si(100) interface shifts downward by ≈3 eV in comparison with that in bulk SiO_2.[15)] The local valence electronic states in the vicinity of the Si^{3+}, Si^{2+}, and Si^{1+} sites at the SiO_2/Si interface, however, have not yet been studied by SXES or EELS. APECS is more suitable than SXES for the study of the Si^{n+} sites at the surface and interface of SiO_2 ultrathin films grown on Si for the following reasons: APECS is more surface-sensitive than SXES, and Auger decay is overwhelmingly predominant over soft-X-ray emission in the Si-2p region. Recently, we investigated the local valence electronic states of Si(100)-2×1[16)] and Si(111)-7×7[17)] clean surfaces by using Si-$L_{23}VV$-Si-2p APECS and discussed, from a surface-site-selective viewpoint, the energy level at which the local density of states (DOS) is the highest and that at which the

*Present address: Department of Chemistry, Faculty of Science, Ehime University, Matsuyama 790-8577, Japan. E-mail: kakiuchi.takuhiro.mc@ehime-u.ac.jp

©2011 The Physical Society of Japan

valence-band maximum (VBM) is found. In the present study, we explore the local valence electronic states of the surface, interface, and substrate for SiO_2/Si(100) by using Si-$L_{23}VV$–Si^{n+}-2p APECS ($n = 0$ for the substrate; 1, 2, 3 for the interface; and 4 for the surface). The results reveal that the local valence states at the Si^{n+} site are shifted downward in binding energy as the nominal oxidation number n increases.

Measurement of the VBM of SiO_2 ultrathin films grown on Si(100) is another important subject because the VBM of a film of sub-nanometer thickness is expected to be different from that of the bulk material and film thickness is a key factor that helps in understanding the leakage current mechanism in MOSFETs. On the basis of scanning tunneling spectroscopy (STS) observations, Nakamura *et al.* reported that the band gap in a thin SiO_2 film [thickness: $\approx$0.3 nm; 1 monolayer (ML) = 1.37 Å][2] grown on Si(111) is approximately 6 eV,[18] which is much smaller than that in SiO_2 bulk ($\approx$8.95 eV). First-principle calculations predict an upward shift of the VBM and a downward shift of the CBM in the quartz SiO_2 region when the distance between the topmost Si layer in the Si(100) substrate and the SiO_2 layer is less than 5 Å.[19] In the present study, we also perform Si-$L_{23}VV$–Si^{4+}-2p APECS measurements for various thicknesses of the SiO_2 film in the case of SiO_2/Si(100). The results indicate that the VBM in a SiO_2 film with a thickness of 1.7–1.5 Å (1.2–1.1 ML) shifts upwards by about 1.6 eV (toward the Fermi level) in comparison with that of a SiO_2 film with a thickness of 13 Å (9.5 ML). This information can be used as a possible guide when manufacturing SiO_2 ultrathin films with low leakage currents.

2. Experimental

SiO_2/Si(100) was prepared by the following procedure. An n-type Si(100) single-crystal wafer with a resistivity of 0.02 Ω cm was mounted at the end of a sample manipulator. A clean Si(100)-2×1 surface was prepared by direct-current heating at temperatures above 1400 K for several seconds and subsequent cooling to room temperature under pressures of less than 3.5×10^{-7} Pa. Then, the clean Si(100)-2×1 surface was exposed to oxygen gas (pressure: 1.3×10^{-4} Pa) at a temperature of 1023 K, for 300, 50, or 25 s. On the basis of Si-2p photoelectron spectra measured at a photon energy ($h\nu$) of 130 eV, the thicknesses of the SiO_2 films on Si(100) were estimated to be approximately 2.8 Å ($\approx$2 ML), 1.7 Å ($\approx$1.2 ML), and 1.5 Å ($\approx$1.1 ML) for exposure times of 300, 50, and 25 s, respectively.[20,21] In addition, SiO_2/Si(100) with a SiO_2 film thickness of 13 Å ($\approx$9.5 ML) was used without further cleaning as the standard amorphous SiO_2 bulk sample.

The samples are irradiated with p-polarized SR with an incidence angle of 84° from the surface normal at beamline 8A (BL-8A) of the SR facility Photon Factory (PF) at KEK. BL-8A is equipped with a soft X-ray monochromator (Zeiss SX-700) and has a typical energy resolution ($E/\Delta E$) of >1000. The spot size on the sample is approximately 6.6 mm × 1.1 mm (width × length). Contamination and charge-up effects on the sample are negligible for every measurement. A self-made coincidence analyzer, which is composed of a coaxially symmetric mirror electron energy analyzer [ASMA, electron energy resolution ($E/\Delta E$) $\approx$ 55], a cylindrical mirror electron energy analyzer (CMA, $E/\Delta E \approx 20$), and a time-of-flight (TOF) ion mass spectrometer,[22] is used for APECS measurements. The procedure for the Si-$L_{23}VV$–Si^{n+}-2p APECS measurement has been described in detail previously.[22] In brief, the CMA is tuned to the Si^{n+} 2p ($n = 0, 1, 2, 3, 4$) photoelectron kinetic energy (*PeKE*), and the ASMA is swept through the Si-$L_{23}VV$ Auger-electron kinetic energy (*AeKE*) region of SiO_2/Si(100). A multichannel scalar is triggered by the Si^{n+}-2p photoelectron signals ($n = 0, 1, 2, 3, 4$), and the Si-$L_{23}VV$ Auger-electron signals are recorded as a function of the TOF difference between the photoelectron and the Auger-electron signals. When a photoelectron and an Auger electron emitted simultaneously are detected, a coincidence signal appears at a specific TOF difference. The integrated coincidence signals plotted as a function of the *AeKE* give the Si-$L_{23}VV$–Si^{n+}-2p APECS spectrum ($n = 0, 1, 2, 3, 4$).

The escape depth of the APECS electrons (ED_{APECS}) is given by

$$\frac{1}{ED_{\mathrm{APECS}}} = \frac{1}{\lambda_{\mathrm{Pe}} \cos\theta_{\mathrm{Pe}}} + \frac{1}{\lambda_{\mathrm{Ae}} \cos\theta_{\mathrm{Ae}}},$$

where λ_{Pe} and λ_{Ae} denote the inelastic mean free paths, and θ_{Pe} and θ_{Ae} denote the acceptance angles for the photoelectron and Auger electron, respectively.[23] Under our experimental conditions, $h\nu$ was 130 eV, while θ_{Pe} and θ_{Ae} of the coincidence analyzer were 28–42° and 48–71°, respectively. Further, λ_{PE} and λ_{AE} were 7.1 Å[20] and 4.8 Å,[24] respectively. We estimated ED_{APECS} to be $\approx$2.0 Å using the above equation. This value was slightly larger than that for a single monolayer of SiO_2 of SiO_2/Si(100) (1.37 Å).[2] Thus, we could mainly probe the topmost surface layers of SiO_2/Si(100) by using Si-$L_{23}VV$–Si^{n+}-2p APECS.

3. Results and Discussion

Figure 1 shows the Si-2p photoelectron spectrum of an SiO_2 ultrathin film with a thickness of 2.8 Å ($\approx$2 ML) grown on a Si(100)-2×1 substrate [2.8-Å SiO_2/Si(100)]. The spectrum is measured by the CMA of the coincidence analyzer, and shown on the relative binding energy where the Si^0-2$p_{3/2}$ peak is taken as the origin. The Si-2p peaks are decomposed into the Si^{n+}-2p photoelectron components ($n = 0, 1, 2, 3, 4$) through a fitting procedure using Voigt functions. The Lorentzian broadening is taken as 0.08 eV, and the Gaussian broadenings, which are mainly governed by the energy resolution of the CMA, are taken as 1.44 eV for all Si^{n+}-2p components. The binding energies relative to the Si^0-2$p_{3/2}$ site are 0.0, 0.8, 1.8, 2.6, and 3.7 eV for Si^0, Si^{1+}, Si^{2+}, Si^{3+}, and Si^{4+}, respectively; these values are in good agreement with those reported in previous studies.[2,20,25,26] The straight dashed lines at −0.3, +0.9, +1.75, +2.63, and +4.1 eV represent the Si^{n+}-2p *PeKE* ($n = 0, 1, 2, 3, 4$) positions taken as the trigger signals for the Si-$L_{23}VV$–Si^{n+}-2p APECS measurements. We choose the Si^{4+}- and Si^0-2p *PeKE* values carefully, so as to suppress other Si^{m+}-2p components ($m \neq 4$ and 0, respectively). Table I shows the spectral weights due to individual Si^{m+}-2p components indicated by the straight dashed lines in Fig. 1. The values approximately correspond to the spectral weights of individual Si^{m+}-$L_{23}VV$ Auger-electron components in the Si-$L_{23}VV$–Si^{n+}-2p APECS spectra.

©2011 The Physical Society of Japan

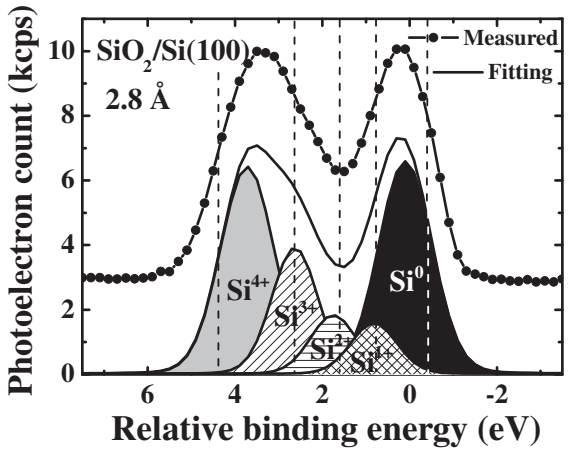

Fig. 1. Si-2*p* photoelectron spectrum measured using the CMA for the 2.8-Å (≈2 ML)-thick SiO_2 ultrathin film thermally grown on Si(100) substrates. The photon energy is 130 eV. The Si^0-$2p_{3/2}$ peak position, which is obtained by curve fitting of the Si-2*p* core-level spectrum measured by the ASMA (not shown), is taken as the origin of the relative binding energy. The shift between the Si^0-$2p_{3/2}$ peak position and the measured highest Si^0-2*p* peak position is about 0.2 eV. The Si-2*p* peaks are decomposed into Si^{n+} components ($n = 0$, 1, 2, 3, and 4) by curve fitting after background subtraction. The straight dashed lines indicate the Si^{n+}-2*p* photoelectron kinetic energy positions taken as the trigger signals for the Si-$L_{23}VV$–Si^{n+}-2*p* APECS measurements.

Table I. The spectral weights due to individual Si^{n+}-2*p* components indicated by the straight dashed lines in the Si-2*p* core-level spectrum of the 2.8-Å SiO_2/Si(100) shown in Fig. 1. The values approximately correspond to the spectral weights of individual Si^{n+}-$L_{23}VV$ Auger-electron components in the Si-$L_{23}VV$–Si^{n+}-2*p* APECS spectra shown in Fig. 2.

Relative binding energy for Si 2*p* (eV)	Si^0 2*p* (%)	Si^{+1} 2*p* (%)	Si^{+2} 2*p* (%)	Si^{+3} 2*p* (%)	Si^{+4} 2*p* (%)
−0.3	98	2	—	—	—
+0.9	64	28	8	—	—
+1.75	12	16	53	19	—
+2.63	—	—	8	68	24
+4.1	—	—	—	1	99

Figures 2(a)–2(e) show the Si-$L_{23}VV$–Si^{n+}-2*p* APECS spectra ($n = 0, 1, 2, 3, 4$) of SiO_2/Si(100) with a thickness of 2.8 Å (≈2 ML) on the relative *AeKE* scale; here, the highest peak (*AeKE* ≈ 87 eV) in the Si-$L_{23}VV$–Si^0-2*p* APECS spectrum [Fig. 2(a)] is taken as the origin. The solid black lines in Figs. 2(a)–2(e) are the noncoincidence Si-$L_{23}VV$ Auger electron spectra of 2.8-Å SiO_2/Si(100) measured simultaneously with each of the Si-$L_{23}VV$–Si^{n+}-2*p* APECS spectra. Hereafter, we will refer to them as "singles Auger electron spectra". The structures of the Si-$L_{23}VV$–Si^{n+}-2*p* APECS spectra ($n = 0, 1, 2, 3, 4$) differ greatly for different values of *n*. The Si-$L_{23}VV$–Si^0-2*p* (Si-$L_{23}VV$–Si^{4+}-2*p*) APECS spectrum corresponds to the Si^0-$L_{23}VV$ (Si^{4+}-$L_{23}VV$) Auger electron spectrum because the Auger electrons emitted from the Si^0 (Si^{4+}) site are measured selectively (see Table I). The Si-$L_{23}VV$–Si^{4+}-2*p* APECS spectrum [Fig. 2(e)] is in good agreement with the previous Si-$L_{23}VV$–Si^{4+}-2*p* APECS spectrum of SiO_2 (thickness: 10 Å)[8] and the noncoincidence Si^{4+}-$L_{23}VV$ Auger electron spectrum of SiO_2 (thickness: ≈1500 Å).[27] The Si-$L_{23}VV$–

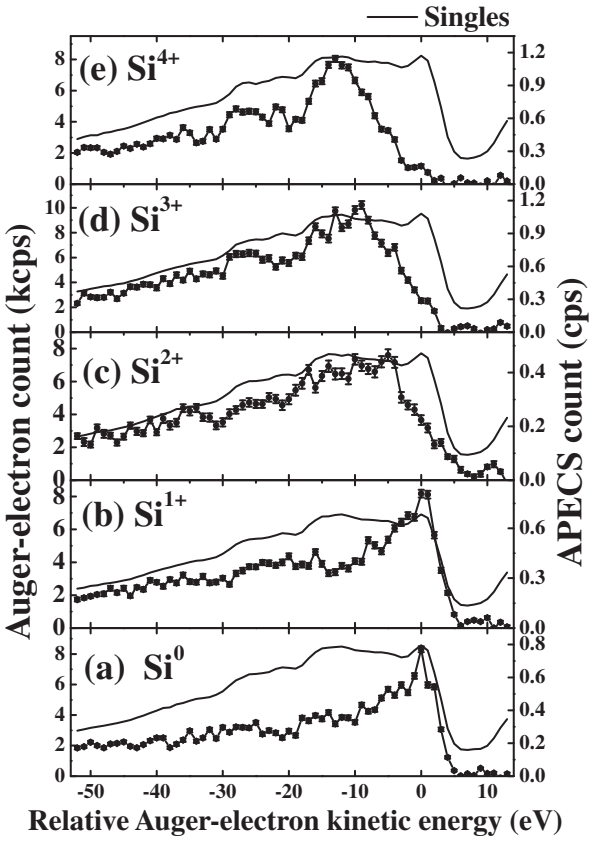

Fig. 2. Si-$L_{23}VV$–Si^{n+}-2*p* APECS spectra of a SiO_2 ultrathin film with a thickness of 2.8 Å grown on Si(100) at $h\nu = 130$ eV [n = (a) 0, (b) 1, (c) 2, (d) 3, and (e) 4]. The solid lines are the singles Auger electron spectra measured simultaneously during each APECS measurement. The accumulation time per datum is (a) 2700, (b) 1800, (c) 1500, (d) 1200, and (e) 1500 s.

Si^0-2*p* APECS [Fig. 2(a)] spectrum resembles the Si-$L_{23}VV$–Si^0-2*p* APECS spectrum of clean Si(100)-2×1.[16] The Si-$L_{23}VV$–Si^{2+}-2*p* (Si-$L_{23}VV$–Si^{3+}-2*p*) APECS spectrum mainly reflects the Si^{2+}-$L_{23}VV$ (Si^{3+}-$L_{23}VV$) Auger electron spectrum because the Auger electrons emitted from the Si^{2+} (Si^{3+}) site are mainly measured (see Table I). These APECS spectra can be used as the fundamental data for surface analysis by Auger electron spectroscopy. The highest peak in the Si-$L_{23}VV$–Si^{n+}-2*p* APECS ($n = 0, 2, 3, 4$) spectra shifts to the lower-relative-*AeKE* side as *n* increases. The highest peak shifts in the Si^{n+}-$L_{23}VV$ Auger electron spectrum are approximately −5, −9, and −13 eV for $n = 2$, 3, and 4, respectively. A small peak is observed at a relative *AeKE* of −2 eV in the Si-$L_{23}VV$–Si^{1+}-2*p* APECS spectrum [Fig. 2(b)]. Since this peak is not observed in the Si-$L_{23}VV$–Si^0-2*p* APECS spectrum [Fig. 2(a)], we state that the highest peak shift in the Si^{1+}-$L_{23}VV$ Auger electron spectrum is about −2 eV. These shift values are useful for surface analysis by scanning Auger electron microscopy.[28]

The Si-$L_{23}VV$–Si^{n+}-2*p* APECS spectra reflect the local density of states (DOS) in the vicinity of the Si^{n+} sites. However, a sophisticated theoretical study is required to obtain the local DOS from the APECS data.[11,12] Instead, we discuss the energy level at which the DOS is the highest in the vicinity of a specific Si site, on the basis of the highest peak in the Si-$L_{23}VV$–Si-2*p* APECS spectra.[16,17] Under the assumption that the hole–hole interaction energy and the

©2011 The Physical Society of Japan

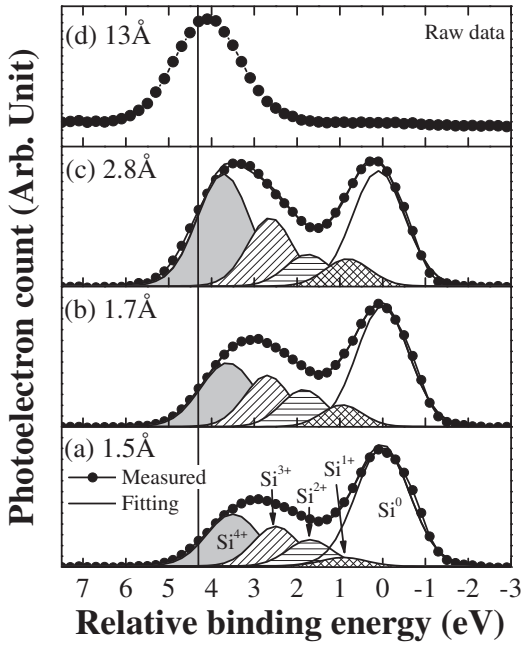

Fig. 3. Si-2*p* photoelectron spectra of (a) 1.5-, (b) 1.7-, (c) 2.8-, and (d) 13-Å SiO_2/Si(100) measured by the CMA. The photon energy is 130 eV. The Si-2*p* peaks of 1.5-, 1.7-, and 2.8-Å SiO_2/Si(100) are decomposed into Si^{n+} components ($n = 0$, 1, 2, 3, and 4) by curve fitting after background subtraction. The straight line indicates the Si^{4+}-2*p* photoelectron kinetic energy position taken as the trigger signal for Si-$L_{23}VV$–Si^{4+}-2*p* APECS measurements.

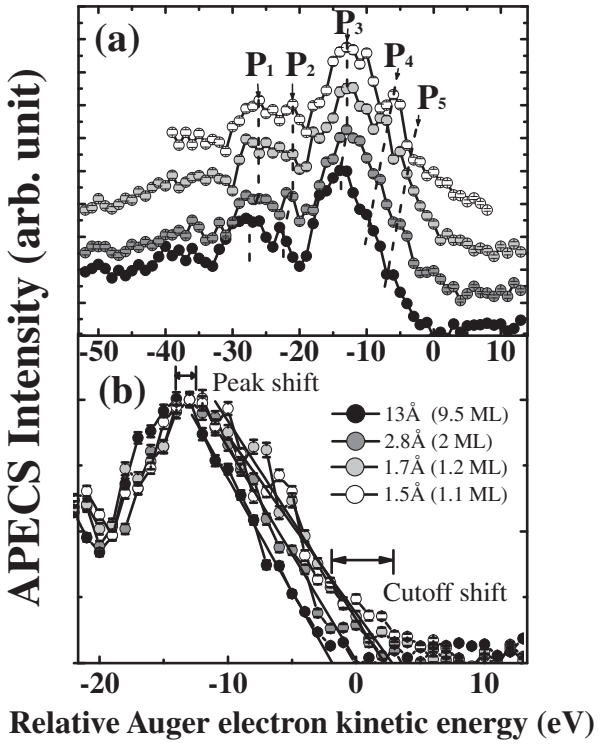

Fig. 4. (a) Thickness dependence of Si-$L_{23}VV$–Si^{4+}-2*p* APECS spectra. The black, gray, light gray, and unfilled circles correspond to SiO_2 thin films with thicknesses of 13, 2.8, 1.7, and 1.5 Å (corresponding to 9.5, 2, 1.2, and 1.1 ML), respectively. The accumulation time per datum is 2100, 1500, 2400, and 1500 s for SiO_2 films with thicknesses of 13, 2.8, 1.7, and 1.5 Å, respectively. (b) The enlarged Si-$L_{23}VV$–Si^{4+}-2*p* APECS spectra. The solid straight lines in the figure represent the least-squares linear fitting between 80% and 20% APECS intensity of the highest peak.

relaxation energy do not depend on the Si site, the difference in binding energy of the valence band at the highest DOS (BE_{VH}) between Si^{n+} and Si^0 sites ($BE_{VH}{}^{n+} - BE_{VH}{}^0$) is given by

$$BE_{VH}{}^{n+} - BE_{VH}{}^0 = \frac{1}{2}[(BE_{2p}{}^{n+} - BE_{2p}{}^0) - (AeKE_{HP}{}^{n+} - AeKE_{HP}{}^0)], \quad (1)$$

in which the superscripts $n+$ and 0 denote the Si^{n+} and Si^0 sites, respectively. The binding energy difference between Si^{n+}-2*p* and Si^0-2*p* ($BE_{2p}{}^{n+} - BE_{2p}{}^0$) can be estimated from the Si-2*p* photoelectron spectrum (see Fig. 1), while the difference in the highest-peak *AeKE* between Si^{n+} and Si^0 ($AeKE_{HP}{}^{n+} - AeKE_{HP}{}^0$) is obtained from the Si-$L_{23}VV$–Si^{n+}-2*p* and Si-$L_{23}VV$–Si^0-2*p* APECS spectra (see Fig. 2). Using eq. (1), we estimate ($BE_{VH}{}^{n+} - BE_{VH}{}^0$) to be approximately −1.4, −3.4, −5.8, and −8.4 eV for $n = 1$, 2, 3, and 4, respectively. Thus, the valence electronic states in the vicinity of the Si^{n+} sites are shifted downward in binding energy as n increases, and this shift is consistent with the downward shift in the binding energy of Si^{n+}-2*p* core-level with an increase in n.

Next, we studied the thickness dependence of the Si-$L_{23}VV$–Si^{4+}-2*p* APECS spectra of SiO_2 ultrathin films grown on Si(100). Figure 3 shows the Si-2*p* photoelectron spectra for SiO_2 films with thicknesses of 13, 2.8, 1.7, and 1.5 Å grown on Si(100) substrates [13-, 2.8-, 1.7-, and 1.5-Å SiO_2/Si(100)]. The Si^{4+}-2*p* peaks in the spectra of 1.5-, 1.7-, and 2.8-Å SiO_2/Si(100) are shifted by 0.7, 0.6, and 0.5 eV with respect to that in the spectrum of 13-Å SiO_2/Si(100), respectively. Figure 4 shows a series of Si-$L_{23}VV$–Si^{4+}-2*p* APECS spectra for 13-, 2.8-, 1.7-, and 1.5-Å SiO_2/Si(100). The highest peak in the Si-$L_{23}VV$–Si^0-2*p* APECS spectrum of 2.8-Å SiO_2/Si(100) is taken as the origin [see Fig. 2(a)]. Every wide-scan Si-$L_{23}VV$–Si^{4+}-2*p* APECS spectrum in Fig. 4(a) shows five peaks (P_1–P_5). The P_1–P_3 peaks shift by ≈1 eV to the higher-*AeKE* side as the SiO_2 film thickness decreases. The shifts of P_1–P_3 are mainly ascribed to final-state effects.[29–31] On the other hand, the P_4 and P_5 peaks shift by ≈4 eV to the higher-*AeKE* side as the SiO_2 thickness decreases. These shifts cannot be explained by the final-state effects because they are much larger than those of P_1–P_3. We therefore ascribe them to the initial-state shift of the local valence electronic states of SiO_2 ultrathin films that accompanies the reduction in SiO_2 thickness.[19] In Fig. 4(b), we show the enlarged S-$L_{23}VV$–Si^{4+}-2*p* APECS spectrum. The lines in Fig. 4(b) are the least-squares linear fitting to the tail of the highest peak in the region with 20–80% intensity. We define the cutoff of *AeKE* ($AeKE_{cutoff}$) as the value corresponding to the point of intersection of the *x*-axis and the fitting line.[16,17] The $AeKE_{cutoff}$ values obtained from each Si-$L_{23}VV$–Si^{4+}-2*p* APECS spectrum are -1.9 ± 0.3, -0.4 ± 0.4, $+2.2 \pm 1.0$, and $+2.2 \pm 0.7$ eV for 13-Å- (9.5-ML-), 2.8-Å- (2-ML-), 1.7-Å- (1.2-ML-), and 1.5-Å- (1.1-ML-) SiO_2/Si(100), respectively. On the basis of these $AeKE_{cutoff}$ data, we can discuss the shift of the *BE* of the VBM (BE_{VBM}) of SiO_2 as a function of the film thickness, because Auger electrons with $AeKE_{cutoff}$ are emitted from the VBM in the vicinity of the Si^{4+} site. Under the assumption that the hole–hole interaction energy and the

©2011 The Physical Society of Japan

relaxation energy do not depend on the thickness of the SiO_2, the BE_{VBM} difference between two samples with different SiO_2 thicknesses ($BE_{VBM}{}^{A} - BE_{VBM}{}^{B}$) is given by the following equation:

$$BE_{VBM}{}^{A} - BE_{VBM}{}^{B} = \frac{1}{2}[(BE_{Si^{4+}\text{-}2p}{}^{A} - BE_{Si^{4+}\text{-}2p}{}^{B}) - (AeKE_{\text{Corrected Cutoff}}{}^{A} - AeKE_{\text{Corrected Cutoff}}{}^{B})], \quad (2)$$

in which the superscripts A and B represent the thickness of SiO_2. In eq. (2), $(BE_{Si^{4+}\text{-}2p}{}^{A} - BE_{Si^{4+}\text{-}2p}{}^{B}) = 0$ for the present case because Si^{4+}-$2p$ photoelectrons with a Si^{4+}-$2p$ *PeKE* of +4.1 eV on the relative *BE* scale are taken as the trigger signals for each SiO_2 thickness (see Fig. 3). $AeKE_{\text{Corrected Cutoff}}$ is the value after the shift due to the final-state effects is corrected. We estimate the shift due to the final-state effects from the shift of the highest peak P_3 of each Si-$L_{23}VV$–Si^{4+}-$2p$ APECS spectrum ($AeKE_{P3}$):

$$AeKE_{\text{Corrected Cutoff}}{}^{A} - AeKE_{\text{Corrected Cutoff}}{}^{B} = (AeKE_{\text{Cutoff}}{}^{A} - AeKE_{\text{Cutoff}}{}^{B}) - (AeKE_{P3}{}^{A} - AeKE_{P3}{}^{B}). \quad (3)$$

From eqs. (2) and (3), we obtain $BE_{VBM}{}^{9.5ML} - BE_{VBM}{}^{2ML} = 0.3 \pm 0.5$ eV, $BE_{VBM}{}^{9.5ML} - BE_{VBM}{}^{1.2ML} = 1.6 \pm 1.1$ eV, and $BE_{VBM}{}^{9.5ML} - BE_{VBM}{}^{1.1ML} = 1.6 \pm 0.8$ eV. The relatively large errors are mainly due to the ambiguity in the $AeKE_{cutoff}$ value; this ambiguity in turn results from the P_4 and P_5 structures. Note that these values mainly reflect the topmost SiO_2 layer, because ED_{APECS} is ≈2.0 Å under the present measurement conditions. These results indicate that the BE_{VBM} values of 1.1- and 1.2-ML SiO_2/Si(100) are shifted upwards by about 1.6 eV (toward the Fermi level) in comparison with that of 9.5-ML SiO_2/Si(100). Assuming that the absolute value of the VBM shift is comparable with that of the CBM, we state that the band-gap narrowing of SiO_2 is about 0.6 eV for 2-ML SiO_2/Si(100) and about 3.2 eV for 1.1- and 1.2-ML SiO_2/Si(100).

The decreased number of Si^{4+} and the increased number of Si^{3+}, Si^{2+}, Si^{1+}, and Si^{0} in the vicinity of the topmost SiO_2 layer are thought to be responsible for the observed VBM shifts in the case of 2.0-, 1.1-, and 1.2-ML SiO_2/Si(100). Since the valence orbitals of Si^{4+} are hybridized with those of the surrounding atoms, the decreased number of neighboring Si^{4+} and the increased number of neighboring Si^{3+}, Si^{2+}, Si^{1+}, and Si^{0} are expected to shift the VBM of the topmost SiO_2 layer to the Fermi level. Yamasaki *et al.* carried out first-principle calculations based on the density functional theory and reported the following. 1) The VBM of (quartz SiO_2)/Si(100) in the region between the topmost Si layer in the Si(100) substrate and a point located 2 Å away from this layer is almost identical to that in the case of the Si(100) substrate; 2) from this point, the VBM begins to shift rapidly and almost saturates at 5 Å; 3) the CBM shows a gradual shift in the transition region; 4) these features are common in (pseudocristobalite SiO_2)/Si(100) and (tridymite SiO_2)/Si(100).[19] Since the thickness of the Si suboxide layer was 3 Å in Yamasaki *et al.*'s calculation, the theoretical features proposed in their study are consistent with our experimental results, according to which the shift of the VBM toward the Fermi level starts at a SiO_2 thickness of about 2.8 Å (2 ML) and reaches 1.6 eV at a thickness of 1.7–1.5 Å (1.2–1.1 ML).

The present results can be used as a possible guide for producing high-quality gate-oxidation films with low leakage currents. Firstly, the thickness of the SiO_2 film should be larger than ≈6 Å (≈4 ML), because band-gap narrowing begins when the distance between the SiO_2 region and the SiO_2/Si interface is about 3 Å. Secondly, the suboxides in the SiO_2 layers should be removed because the presence of these suboxides reduces the band gap not only at the suboxides but also at the neighboring SiO_2 sites. Thus, suboxides in a gate-oxidation film may contribute to the formation of a leakage current path.

4. Conclusions

We have measured Si-$L_{23}VV$ Auger-electron Si^{n+}-$2p$ ($n = 0, 1, 2, 3, 4$) photoelectron coincidence spectra of ultra-thin SiO_2 films [thickness: 2.8 Å (≈2.0 ML)] that are thermally grown on Si(100)-2×1. The results indicate that the binding energy of the valence band at the highest DOS (BE_{HV}) of the Si^{n+} site ($n = 0, 1, 2, 3, 4$) shifts downwards as n increases. The shift of BE_{HV} from Si^{0} to Si^{n+} is estimated to be approximately −1.4, −3.4, −5.8, and −8.4 eV for $n = 1$, 2, 3, and 4, respectively. We have also measured Si-$L_{23}VV$–Si^{4+}-$2p$ APECS spectra of SiO_2/Si(100) as a function of SiO_2 film thickness. The results indicate that the binding energy of the VBM (BE_{VBM}) of SiO_2 films with thicknesses of 2.8, 1.7, and 1.5 Å (2, 1.2, and 1.1 ML) shifts upwards by approximately 0.3 ± 0.5, 1.6 ± 1.1, and 1.6 ± 0.8 eV, respectively (toward the Fermi level), in comparison with that in the case of SiO_2 film with a thickness of 13 Å (9.5 ML). The BE_{VBM} shifts are attributed to the decreased number of Si^{4+} and the increased number of Si^{3+}, Si^{2+}, Si^{1+}, and Si^{0} in the vicinity of the topmost SiO_2 layer. These results can be used as a possible guide for the production of high-quality gate-oxidation films with low leakage currents.

Acknowledgments

We express our sincere thanks to the members of the Photon Factory for their invaluable help during the experiments. This research was supported by PRESTO (Structure Function and Measurement Analysis) from the Japan Science and Technology Agency (JST). This research was performed with the approval of the Photon Factory Program Advisory Committee (PF PAC No. 2006S2-002).

1) H. Watanabe, K. Kato, T. Uda, K. Fujita, M. Ichikawa, T. Kawamura, and K. Terakura: Phys. Rev. Lett. **80** (1998) 345.
2) J. H. Oh, H. W. Yeom, Y. Hagimoto, K. Ono, M. Oshima, N. Hirashita, M. Nywa, A. Toriumi, and A. Kakizaki: Phys. Rev. B **63** (2001) 205310.
3) T. Yamasaki, K. Kato, and T. Uda: Phys. Rev. Lett. **91** (2003) 146102.
4) H. Kageshima and K. Shiraishi: Phys. Rev. Lett. **81** (1998) 5936.
5) A. Stesmans and V. V. Afanas'ev: J. Appl. Phys. **83** (1998) 2449.
6) H. W. Haak, G. A. Sawatzky, and T. D. Thomas: Phys. Rev. Lett. **41** (1978) 1825.
7) E. Jensen, R. A. Bartynski, S. L. Hulbert, E. D. Johnson, and R. Garrett: Phys. Rev. Lett. **62** (1989) 71.
8) G. Stefani, R. Gotter, A. Rucco, F. Offi, F. Da Pieve, S. Iacobucci, A. Morgante, A. Verdini, A. Liscio, H. Yao, and R. A. Bartynski: J. Electron Spectrosc. Relat. Phenom. **141** (2004) 149.
9) G. A. van Riessen, S. M. Thurgate, and D. E. Ramaker: J. Electron Spectrosc. Relat. Phenom. **161** (2007) 150.

©2011 The Physical Society of Japan

10) G. van Riessen, Z. Wei, R. S. Dhaka, C. Winkler, F. O. Schumann, and J. Kirschner: J. Phys.: Condens. Matter **22** (2010) 092201.
11) E. Jensen, R. A. Bartynski, M. Weinert, S. L. Hulbert, E. D. Johnson, and R. F. Garrett: Phys. Rev. B **41** (1990) 12468.
12) R. A. Bartynski, S. Yang, S. L. Hulbert, C.-C. Kao, M. Weinert, and D. M. Zehner: Phys. Rev. Lett. **68** (1992) 2247.
13) K. Hirose, H. Nohira, K. Azuma, and T. Hattori: Prog. Surf. Sci. **82** (2007) 3.
14) Y. Yamashita, S. Yamamoto, K. Mukai, J. Yoshinobu, Y. Harada, T. Tokushima, T. Takeuchi, Y. Takata, S. Shin, K. Akaki, and S. Tsuneyuki: Phys. Rev. B **73** (2006) 045336.
15) D. A. Muller, T. Sorsch, S. Moccio, F. H. Baumann, K. Evans-Lutterodt, and G. Timp: Nature **399** (1999) 758.
16) T. Kakiuchi, S. Hashimoto, N. Fujita, M. Tanaka, K. Mase, and S. Nagaoka: J. Phys. Soc. Jpn. **79** (2010) 064714.
17) T. Kakiuchi, M. Tahara, S. Hashimoto, N. Fujita, M. Tanaka, K. Mase, and S. Nagaoka: Phys. Rev. B **83** (2011) 035320.
18) Y. Nakamura, Y. Nagadomi, K. Sugie, N. Miyata, and M. Ichikawa: J. Appl. Phys. **95** (2004) 5014.
19) T. Yamasaki, C. Kaneta, T. Uchida, T. Uda, and K. Terakura: Phys. Rev. B **63** (2001) 115314.
20) F. J. Himpsel, F. R. McFeely, A. Taleb-Ibrahimi, J. A. Yarmoff, and G. Hollinger: Phys. Rev. B **38** (1988) 6084.
21) W. K. Choi, F. W. Poon, F. C. Loh, and K. L. Tan: J. Appl. Phys. **81** (1997) 7386.
22) T. Kakiuchi, E. Kobayashi, N. Okada, K. Oyamada, M. Okusawa, K. K. Okudaira, and K. Mase: J. Electron Spectrosc. Relat. Phenom. **161** (2007) 164.
23) T. Kakiuchi, S. Hashimoto, N. Fujita, M. Tanaka, K. Mase, and S. Nagaoka: Surf. Sci. **604** (2010) L27.
24) S. Tanuma, C. J. Penn, and D. R. Penn: Surf. Interface Anal. **17** (1991) 927.
25) H. W. Yeom, H. Hamamatsu, T. Ohta, and R. I. G. Uhrberg: Phys. Rev. B **59** (1999) R10413.
26) F. Jolly, F. Rochet, G. Dufour, C. Grupp, and A. Taleb-Ibrahimi: J. Non-Cryst. Solids **280** (2001) 150.
27) D. E. Ramaker, J. S. Murday, N. H. Turner, G. Moore, M. G. Lagally, and J. Houston: Phys. Rev. B **19** (1979) 5375.
28) M. Prutton and M. M. El Gomati eds.: *Scanning Auger Electron Microscopy* (Wiley, Chichester, U.K., 2006).
29) A. Pasquarello, M. S. Hybertsen, and R. Car: Phys. Rev. B **53** (1996) 10942.
30) J. L. Alay, M. Fukuda, C. H. Bjorkman, K. Nakagawa, S. Yokoyama, S. Sasaki, and M. Hirose: Jpn. J. Appl. Phys. **34** (1995) L653.
31) Th. Eickhoff, V. Medicherla, and W. Drube: J. Electron Spectrosc. Relat. Phenom. **137–140** (2004) 85.

©2011 The Physical Society of Japan